

Contribution of seismic and acoustic methods to the characterization of karstic formations

J.-L. Mari, G. Porel

5.1 Introduction

Over the past decade, many underground aquifers have been developed as experimental sites. These sites are designed for in situ measurements and calibration of flow, transport and/or reactions in underground reservoirs that are heterogeneous by nature.

This chapter of *Well seismic surveying and acoustic logging* is published under Open Source Creative Commons License CC-BY-NC-ND allowing non-commercial use, distribution, reproduction of the text, via any medium, provided the source is cited.

© EDP Sciences, 2018

DOI: 10.1051/978-2-7598-2263-8.c007

One such Hydrogeological Experimental Site (HES) was built by the University of Poitiers (France) near its campus, for the purpose of providing facilities to develop long-term monitoring and experiments for a better understanding of flow and transfers in fractured rocks [2], [3], [4], [5].

After a brief review of the geological context, this chapter shows the contribution of seismic and acoustic methods to the characterization of a karstic carbonate reservoir. The different geophysical methods studied are:

- 3D surface seismic method
- Well seismic methods: ambient noise measurements and Vertical Seismic Profiles (VSP) survey
- Acoustic method: full waveform acoustic logging

This chapter shows the value of combining different geophysical methods to describe geological formations at different scales to detect karstic bodies and to quantify flows.

5.2 Geological context

The aquifer studied is 20 to 130 m in depth and consists of tight karstic carbonates of Middle Jurassic age. It lies on the borderline, called the “Poitou threshold”, between the Paris and the Aquitaine sedimentary basins (Figure 5.1). The Hydrogeological Experimental Site (HES) covers an area of 12 hectares over which 35 wells were drilled to a depth of 120 m (Figure 5.1). The top of the reservoir was flat and horizontal 150 million years ago, before being eroded and weathered during the Cretaceous and Tertiary ages. Today the reservoir top is shaped with hollows and bumps with a magnitude reaching up to 20 m.

The site construction phase started in 2002 and to date 35 wells have been bored over the whole thickness of the reservoir. Most wells are fully documented, with drilling records and logs of various types, including gamma ray, temperature, and acoustic logs. In addition, two wells were entirely cored.

Hydrogeological investigations show that maximum pumping rates vary from well to well and range from 5 to 150 m³/h. However, the aquifer responds fairly evenly to the hydraulic stress of a pumped well. This is assumed to be the consequence of a local karstic flow in open conduits. The presence of karstic drains is supported by recent well logs using optic (OPTV) or acoustic (BHTV) imaging. Almost all wells have shown caves and conduits that were intersected by the walls of the boreholes, with average apertures sometimes in the range of 0.2 to 0.5 m.

These conduits are mostly enclosed in three thin horizontal layers at depths of 35 m, 88 m and 110 m. Of course, these layers are intercepted by vertical wells and this potentially results in a good connection between wells and karstic drains. This connection is mainly controlled by the degree to which drains are re-opened

in the vicinity of the well. The hydraulic slug tests show in some cases a very rapid propagation of the pressure wave over large distances (up to more than 100 m). These observations have enabled the mapping of a diffusivity distribution and illustrated the important connections between the wells (Figure 5.1, bottom). Preferential connections are visible along the N90 direction (wells M13-M21-M22-M19 and wells M04-M06-M11). Ultimately it was considered crucial to better define the geometry of the reservoir with a resolution compatible with both the scale of a well, and also with the scale of the entire experimental site. It was decided that high-resolution geophysical tools are well designed to undertake this kind of investigation.

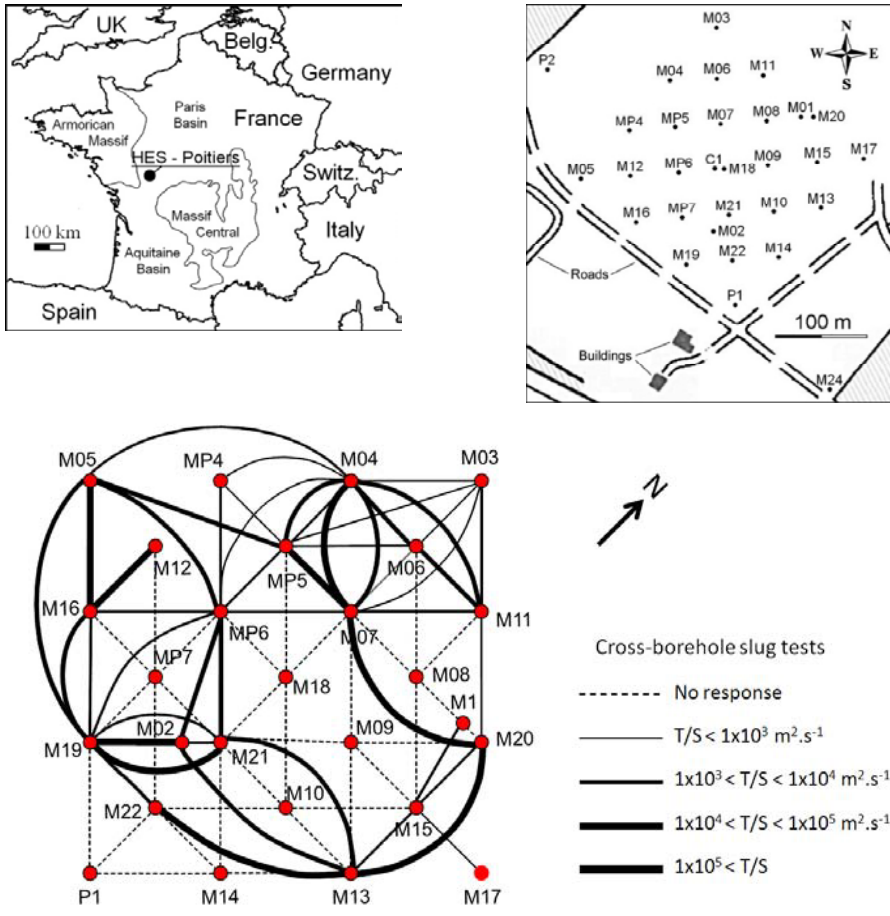


Figure 5.1 Hydrogeological Experimental Site in Poitiers. Top: site map and well locations. Bottom: diffusivity map from slug test.

5.3 3D seismic acquisition and processing

Due to the limitations of the studied area, the length of the seismic line could not exceed 250 m in the in-line direction. The extension of the area is 300 m in the cross-line direction, perpendicular to the in-line direction of the lines. As a result, 20 receiver lines were implemented, with a 15 m distance between adjacent lines.

Figure 5.2 (top left) shows a map of the seismic lines and wells. Data acquisition was made with a 48 channel recorder and a single geophone (10 Hz) per trace. An explosive source (25 g) was detonated, making it easy to identify and select first arrivals.

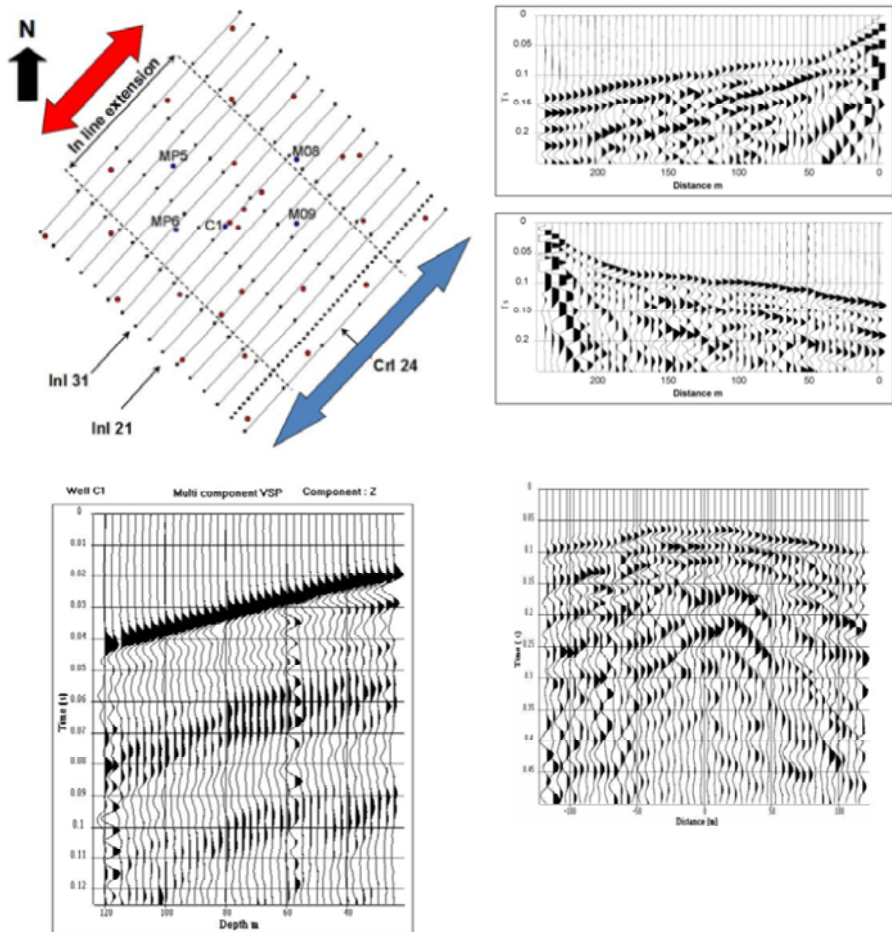


Figure 5.2 3D seismic acquisition. Top left: Seismic line implementation and well location (red points). Top right: Example of direct and reverse in-line shot points. Bottom left: Vertical seismic profile (VSP) at well C1. Bottom right: example of cross-line shot point.

A 5 m distance between two adjacent geophones was selected to avoid any spatial aliasing. A direct shot and a reverse shot were recorded per receiver line (“in-line” shots). Figure 5.2 (top right) shows an example of an in-line direct and reverse shot gather. Three shot points in the cross-line direction were fired at distances of 40 m, 50 m and 60 m from the receiver line under consideration. Figure 5.2 (bottom right) shows an example of a cross-line shot gather. The range of offsets was selected to optimize the quality of the seismic image over the reservoir depth interval, i.e. between 40 m and 130 m. A 40 m minimum offset distance was chosen to reduce the influence of the surface waves. The time sampling interval was 0.25 ms and the recording length was 0.5 s.

The processing sequence has been described in detail in several publications (Mari & Porel [1] and Mari & Delay [6]), so it is only briefly explained here. Each shot point was processed independently (both in the cross-line direction and in the in-line direction) to obtain a single-fold section with a sampling interval of 2.5 m (half the distance between 2 adjacent geophones) in the in-line direction. The processing of an in-line direct and reverse shot gather has enabled a single-fold section with an in-line extension of 240 m to be obtained (indicated by a blue arrow on the seismic line map) while a cross-line shot gather has provided a single-fold section with an in-line extension of 120 m (indicated by a red arrow on the seismic lines map).

A 3D seismic refraction tomography [7] was carried out to map the irregular shape of the top of the karstic reservoir and to obtain static corrections and a velocity model of the overburden. To add information to the inversion procedure, we used in-line and cross-line cross shots simultaneously, with an offset of 60 m. The shots were selected to ensure that the refracted wave was the first arrival wave, regardless of the source receiver distance. The picked times of the first seismic arrivals for all shots (in-line and cross-lines shots), the depth map of the top of the reservoir (defined from the wells) and the velocity model obtained by the Plus–Minus [8] method were used as input data for the inversion procedure. The inversion results obtained with 3D data emphasize the previously mentioned geological structures [9], providing a better understanding of their alignments and shape (corridor of fractures). Furthermore, no cavities were detected near the surface.

The processing sequence includes: amplitude recovery, deconvolution, wave separation (SVD method for extracting refracted waves and combining the SVD and F-K methods for filtering surface waves), static corrections (obtained by inversion tomography) and normal move-out (NMO) corrections. A VSP was recorded in well C1 (Figure 5.2, bottom left). VSP data were processed to obtain a time versus depth relationship and a velocity model. The velocity model has been used to apply the NMO corrections. The VSP time versus depth law was also used to convert the time sections into depth sections with a 0.5 m depth sampling interval. The single-fold depth sections were merged to create the 3D block. The width of the block in the in-line direction is 240 m, and 300 m in the cross-line direction.

In the in-line direction, the abscissa zero indicates the location of the source line. The abscissa of the reflecting points varies between -120 m and 120 m in the in-line direction. The distance between two reflecting points is 2.5 m. In the cross-line

direction, the distance between two reflecting points is 5 m. The depth sections were deconvolved to increase the vertical resolution. They were then integrated to transform a 3D amplitude block into a pseudo velocity block, using velocity functions (sonic logs recorded at wells C1, MP5, MP6, M08, M09) as constraints. The pseudo velocity sections of the 3D block thus obtained were merged with those obtained by refraction tomography to create a 3D extended velocity model from the surface (Figure 5.3).

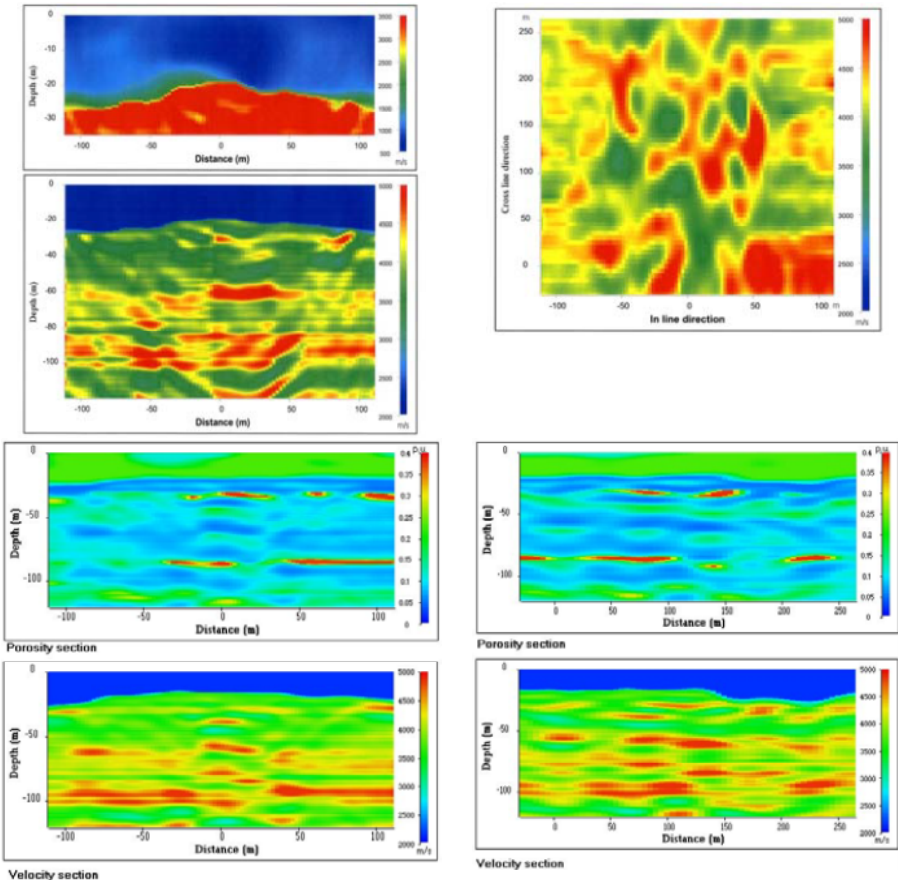


Figure 5.3 3D seismic processing. Top left: in-line 31 pseudo-velocity section (upper part: zoom of 0 to 35 m depth interval). Top right: pseudo-velocity map at 87 m depth. Bottom left: in-line 21 pseudo-velocity and porosity seismic sections. Bottom right: cross-line 24 pseudo-velocity and porosity seismic sections.

Figure 5.3 top left shows the results obtained for the in-line 31 seismic section extracted from the 3D extended velocity model. It also shows the velocity map at a depth of 87 m (Figure 5.3 top right). The 3D velocity model shows the large

heterogeneity of the aquifer reservoir in the horizontal and vertical planes. To quantify the porosity variations within this aquifer, the seismic interval velocities were first converted into resistivity values. For this purpose, the empirical relationship between seismic velocity and resistivity proposed by Faust [10] was used. Resistivity values were then converted into porosity values, using Archie's law [11]. Figure 5.3 (bottom) shows the pseudo velocity and porosity seismic sections for the in-line 21 and cross-line 24.

The resulting 3D seismic pseudo-porosity block revealed three high-porosity layers, at depths of 35 to 40 m, 85 to 87 m and 110 to 115 m. The 85 to 87 m layer is the most porous, with porosities higher than 30 %, which represents the karstic part of the reservoir. Figure 5.4 shows the distributions of porous bodies in the 80 to 90 m and 100 to 120 m depth intervals.

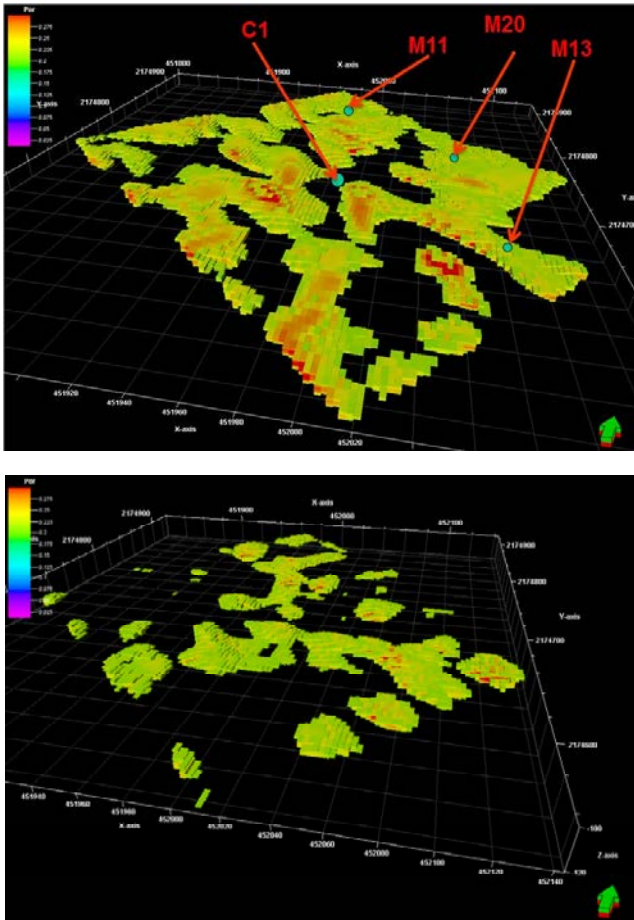


Figure 5.4 Distribution of karstic bodies. Top: in the 80 to 90 m depth interval. Bottom: in the 100 to 120 m depth interval.

The 3D block is composed of elementary cells (2.5 m in the in-line direction, 5 m in the cross-line direction, and 1 m deep), which clearly show the connectivity of the karstic bodies. The local validation of the results obtained by the 3D seismic method was achieved using full waveform acoustic data and VSP, recorded in 11 wells in 2014 and 2015 respectively. Acoustic logging and VSP have higher vertical resolution than the 3D seismic method, however, their lateral investigation was restricted to the vicinity of the well. 11 wells were selected: C1, M03, M05, M11, M13, M14, M20, M22, MP5, MP6 and MP7.

In this chapter, we show the results obtained from wells C1, M11, M13 and M20. The well locations are indicated in Figures 5.1 and 5.4.

5.4 Well seismic measurements

For VSP acquisition, the seismic source was a lightweight drop and the borehole sensor was a hydrophone. The sampling interval depth was 2.5 m. Before each shot, the ambient noise was recorded. The VSPs were highly corrupted by Stoneley waves (tube waves). The conversion of down-going P-waves into up-going Stoneley waves was observed at the level of the karstic bodies. This phenomenon occurs in highly permeable formations.

Figure 5.5 shows the data recorded at well C1. The phenomenon of the conversion of P-waves into Stoneley waves can be identified at a depth of 60 m (Figure 5.5, top right). Indeed, it can be observed that the first arrival, which is the down-going P-wave, is highly attenuated at a depth of 60 m. At this depth, the P-wave is partly converted into a down-going Stoneley wave, which is reflected at the bottom of the well. The VSP data were processed to extract the down-going and up-going Stoneley waves. The down-going Stoneley wave can be extracted using a velocity filter, the velocity being the apparent velocity of the Stoneley wave. A narrow-band wavenumber filter applied after the velocity correction is equivalent to a velocity filter in the f, k domain. The velocity was determined with a velocity scan. For a given velocity value, the Stoneley wave and residue are extracted, the difference between the initial VSP data and the estimated down-going Stoneley wave was calculated. The selected velocity was the velocity that minimized residues. The apparent velocity of the Stoneley mode is about 1,300 m/s. The same procedure was applied to extract the up-going Stoneley wave, but the apparent velocity was negative.

A Hilbert transform was applied to the different wave fields to estimate their amplitude (instantaneous envelope). Figure 5.5 (bottom left) shows the increase in amplitude of the Stoneley waves. The instantaneous amplitudes of the up-going Stoneley waves were stacked in a small corridor located after the arrival time of the down-going P-wave, to obtain a body wave to Stoneley wave conversion factor (Figure 5.5, bottom right), which relates to a karstic level at 57 m in depth.

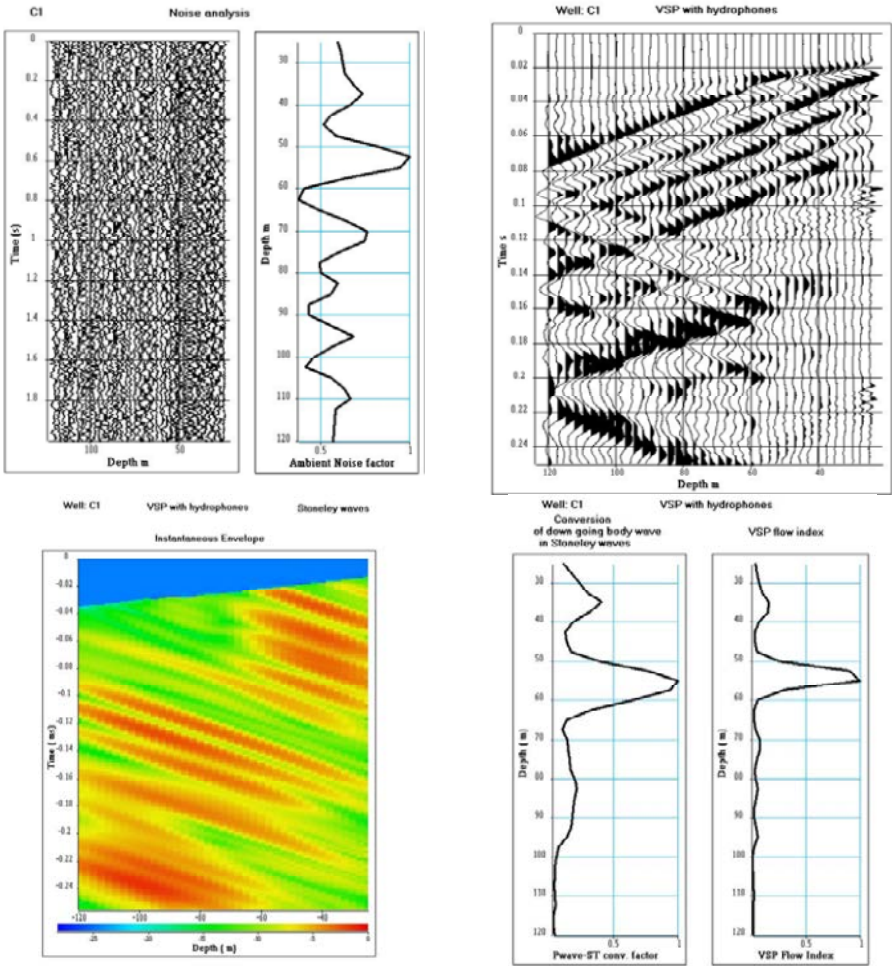


Figure 5.5 Flow detection using both ambient noise measurement and VSP data at well C1. Top left: Ambient noise and ambient noise factor. Top right: VSP data showing a high level of Stoneley waves. Bottom left: Up-going Stoneley waves (instantaneous envelope). Bottom right: P-wave to Stoneley wave conversion factor and VSP flow index.

Assuming that flow circulation in the karstic network generates a rise in ambient noise [12], the analysis of the seismic noise was carried out to detect the presence of flows [13]. For this purpose, the average and the variance of the amplitude spectrum of each noise trace was calculated. We noted a significant increase in the ambient noise factor, defined as the relationship between the average and the variance of the spectrum, at the level of karstic bodies. The analysis of the ambient noise therefore shows that the variations of the ambient noise factor correlate with the level of

conversion of P-waves into Stoneley waves. Figure 5.5 (top left) shows the ambient noise and its associated ambient noise factor. The attribute, named VSP flow index, defined as the product of the ambient noise factor by the body wave to Stoneley wave conversion factor (Figure 5.5, bottom right) was used to detect both karstic bodies and flow.

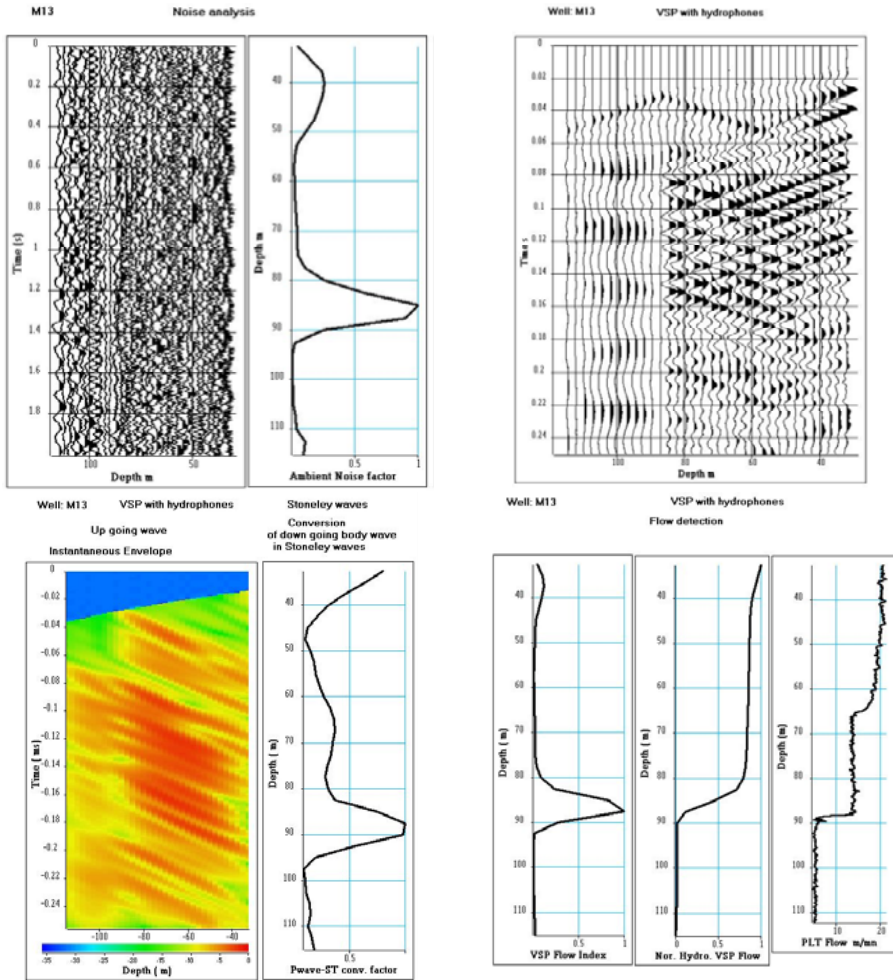


Figure 5.6 Flow detection using both ambient noise measurement and VSP data at well M13. Top left: Ambient noise and ambient noise factor. Top right: VSP data showing a high level of Stoneley waves. Bottom left: Up-going Stoneley waves and P-wave to Stoneley wave conversion factor. Bottom right: Detection of flow at 87 m deep and comparison of VSP flow with PLT flow.

The analysis of ambient noise and of the increase in the P-body waves to Stoneley waves conversion is currently the only method available to detect the flow in this C1 well. Due to the small borehole diameter, it was not possible to run BHTV and PLT logs in well C1. However, the karstic level at a depth of 57 m was confirmed by acoustic logging.

The same procedure was therefore applied to the dataset recorded in well M13 (Figure 5.6).

Figure 5.6 shows:

- Top left: the ambient noise and its associated noise factor, which detects a karstic body between 85 and 87 m, and predicts a flow.
- Top right: The VSP data. A down-going Stoneley wave reflected at a depth of 85 m can be noted. The conversion of the down-going P-wave into an up-going and down-going Stoneley wave can also be observed at the same depth.
- Bottom left: The instantaneous amplitude of the up-going Stoneley waves and the associated conversion factor between the P-wave and the Stoneley wave, which confirms the presence of a karstic body between 85 and 90 m.
- Bottom right: the VSP flow index, which predicts a flow between 85 and 87 m. The VSP flow index has been integrated in depth from bottom to top to mimic a flowmeter in order to compare with a PLT log. A good correlation between the 2 logs can be noted, taking into account that the vertical resolution is not the same for the 2 logs (2.5 m for the VSP, and 1 cm for the PLT).

The flow variation of the PLT log at 65 m deep is due to a change of the borehole diameter.

5.5 Monopole full waveform acoustic logging

The transmission of an acoustic wave through geological formations is used for formation characterization. Monopole-type tools are the most commonly used for this purpose.

Monopole sources and receivers are multidirectional. Sources generate compression in the fluid, creating in the formation a compression wave (P-wave) and a shear wave (S-wave) at the refraction limit angles. In a vertical well, these tools are used to record five propagation modes: the refracted compression wave; the refracted shear wave (only in fast formations); the fluid wave; and two dispersive guided modes – the pseudo Rayleigh waves (only in fast formations) and the Stoneley waves. Acoustic logging enables the measurement of vertical propagation velocities and the frequencies of the different waves recorded.

The analysis of the acoustic waves recorded on each receiver of the logging tool is used to calculate additional logs, defined as acoustic attributes, useful for the characterization of the formation, such as: amplitude, shape index, wavelength

and attenuation logs. The acoustic tool used for the field experiment was a flexible monopole tool with two far offset receivers (3 m (R1) and 3.25 m (R2) offsets).

At the level of a karstic body, we observed a strong attenuation of the refracted P-wave and a distortion of the acoustic signal that made it difficult to pick the refracted P-wave arrival times. Processing based on Singular Value Decomposition (SVD, [14]) was carried out independently on the 2 offset sections. The refracted wave signal space was given by the first Eigen section obtained by SVD:

$$\underline{I}^{\text{sig}} = \lambda_1 \underline{u}_1 \underline{v}_1^T \quad 1$$

v_1 is the first singular vector giving the time dependence, and it is therefore named the normalized wavelet, u_1 is the first singular vector giving the amplitude in depth, and is therefore called the propagation vector and λ_1 the associated eigenvalue. The amplitude variation of the refracted wavelet over the depth interval is $\lambda_1 u_1$.

A cost function based on the correlation of normalized wavelets V_1 extracted from the two constant offset sections enables the simultaneous calculation of the velocity V of the formation, and the correlation coefficient between the wavelets.

SVD processing leads to the calculation of a specific attribute used to detect karstic levels. The attribute, called the Noise/Signal detector, is the product of 3 normalized terms:

- A velocity term: $CV = 1 - (V/V_{\text{max}})$. The lower the velocity, the higher the velocity term. In karstic zones, a high CV coefficient is observed.
- An amplitude term: $CA = 1 - (A/A_{\text{max}})$, with $A = \lambda_1 \underline{u}_1$. In karstic zones, a high CA coefficient is observed.
- A correlation term: $CCor = 1 - (Cor/Cor_{\text{max}})$, Cor being the correlation coefficient between two normalized wavelets. In karstic zones, a high CCor coefficient is observed.

Figure 5.7 shows the acoustic data from well M13. On the 3 m constant offset section, we can clearly see:

- the refracted P-waves between 0.5 and 1 milliseconds,
- the converted refracted shear waves between 1.2 and 1.8 milliseconds,
- the Stoneley modes after 2 milliseconds.

One can notice a strong attenuation of all waves between 85 and 90 m, highlighted by the Noise/Signal detector log. The BHTV log confirms the presence of a karstic layer. The results are consistent with the seismic measurements (VSP flow index) and PLT flow (Figure 5.6).

Figure 5.8 compares BHTV log, VSP flow index, Noise/Signal detector (acoustic logging) and PLT flow at well M11. A karstic body with a flow was clearly detected between 85 and 90 m.

5. Contribution of seismic and acoustic methods to the characterization of karstic formations

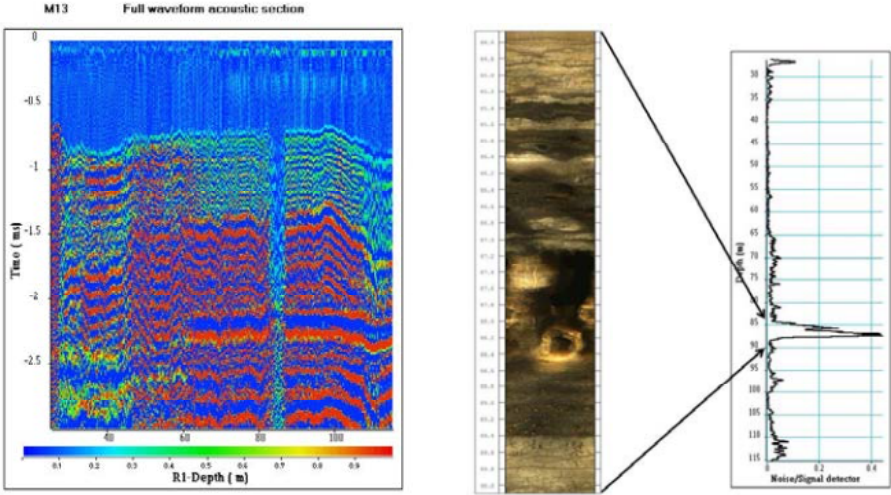


Figure 5.7 Acoustic data at well M13. Acoustic section (left) and comparison between BHTV and noise/signal detector (right).

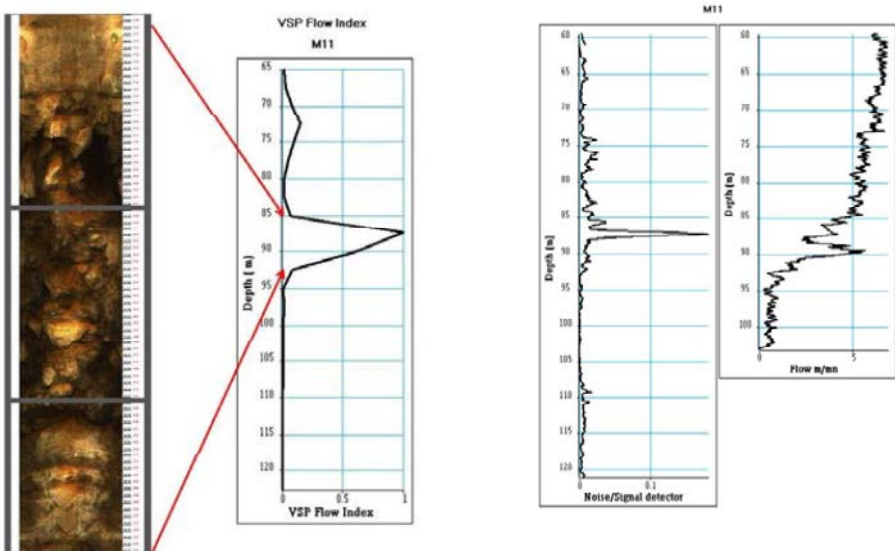


Figure 5.8 Flow detection at well M11. Comparison between BHTV, VSP flow index, noise/signal detector (acoustic logging) and PLT.

Figure 5.9 is a synthesis of the methods developed to detect karstic bodies and to quantify flows. It gathers data from acoustic logging, ambient seismic noise, VSP data, OPTV and PLT flow metering.

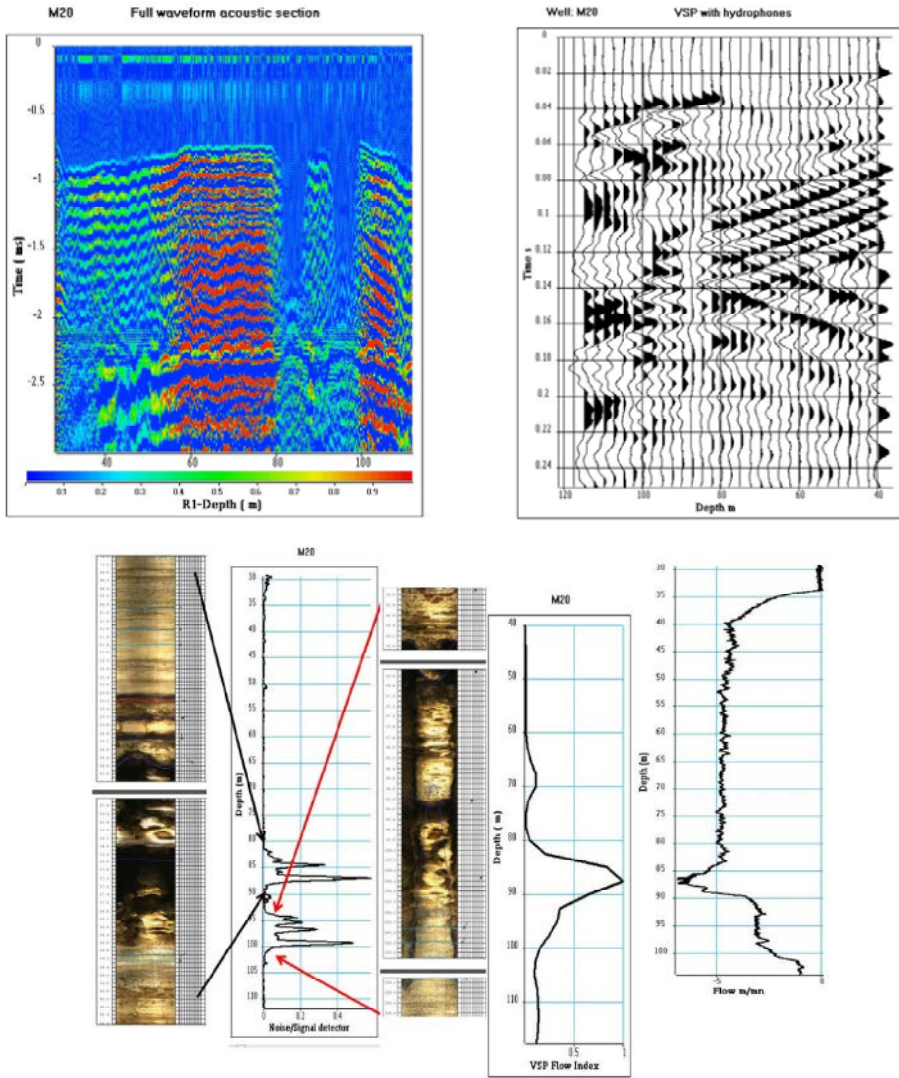


Figure 5.9 Flow detection at well M20. Top: Full waveform acoustic data (left) and VSP data (right). Bottom: comparison between OPTV, Noise/signal detector (acoustic data), VSP flow index and PLT log.

Regarding the data recorded in well M20, the 3 m constant-offset acoustic section shows:

- the refracted P-waves between 0.5 and 1 milliseconds
- locally, the converted refracted shear waves between 1.2 and 1.8 milliseconds
- the fluid waves characterized by very high frequencies in the order of 30 kHz
- the Stoneley wave modes

An analysis of the acoustic data and the calculations made from the Noise/Signal detector have enabled the detection of karstic levels in two depth intervals between 82 and 88 m and between 95 and 100 m. In these intervals the acoustic section shows a strong attenuation of the refracted P-wave. The presence of the 2 karstic layers was validated by the OPTV logs.

The VSP shows a down-going Stoneley mode which is strongly attenuated at 82.5 m deep. The phenomena of a conversion from a down-going P-wave to Stoneley waves can be observed between 82.5 and 100 m. The processing of VSP data and the ambient noise analysis confirmed that the 82.5 to 100 m depth interval is a karstic layer and detect the presence of flow. A PLT log obtained during pumping in well M04 validates the results of the acoustic-seismic experimentation.

5.6 Conclusion

This chapter has shown the benefit of combining different geophysical methods to describe geological formations at different scales. The aquifer studied, 20 to 130 m in depth, consists of tight karstic carbonates.

In 2004, a seismic reflection and refraction survey was carried out on the study site [1]. An analysis of the seismic refraction tomography was made to calculate the velocity distribution in the karst aquifer cover, and to map the top of this reservoir. The 3D seismic data were processed to obtain, following inversion, the distribution of the seismic velocities in the reservoir. The result was a high-resolution 3D seismic block. This enables the identification of three high-porosity, presumably water-producing layers, at depths of 35 to 40 m, 85 to 87 m and 110 to 115 m. The 85 to 87 m deep layer is the most porous, with porosities of over 30 %, which represents the karstic part of the reservoir.

To locally validate the results obtained by the 3D seismic method, full waveform acoustic data and VSP were recorded in 11 wells, VSP and acoustic methods having a higher vertical resolution than the surface seismic method.

A methodology has been developed to detect flow using both ambient noise measurement and VSP data recorded with a hydrophone sensor. The VSP, recorded in water wells, were highly corrupted by Stoneley waves (tube waves). Conversion of the down-going P-waves into Stoneley waves was observed at the level of the karstic bodies. This phenomenon occurs in highly permeable formations. The analysis of the ambient noise shows that the variations of its characteristics (spectral variance)

are correlated with the conversion level of P-waves into Stoneley waves. An attribute, the VSP flow index, was calculated to detect both karstic levels and flows.

Full waveform acoustic data were recorded both to locally validate the results obtained by the seismic methods (3D and VSP) and to evaluate the potential of the acoustic method to detect karstic bodies with a very high resolution (0.25 m deep). A methodology has also been developed to process the acoustic data generated by the flows in the karst conduits. The methodology is based on Singular Value Decomposition processing, which is used to estimate simultaneously the velocity of the formation, the amplitude of the acoustic signal, and the level of noise. An attribute, called the Noise/Signal detector, was calculated to detect karstic levels.

The seismic (3D, VSP) and acoustic data were compared with OPTV logging data and PLT data. The flows predicted by seismic methods were confirmed by PLT data.

The conclusions of the study are:

- The 3D seismic block can be used to build a 3D model of karst aquifers,
- Conversion of P-waves into Stoneley waves was observed in the VSP data at the top of the producing levels,
- The variations of the spectral characteristics of the ambient noise are strongly correlated with flow measurements (PLT) and the conversion of P-waves to Stoneley waves,
- Analysis of ambient noise and conversion of body waves into Stoneley waves could also be used to detect flow circulation.

Therefore, we can conclude that 3D seismic, full waveform acoustic logging and VSP enable the description of karstic formations at different scales.

5.7 Acknowledgements

We thank the University of Poitiers for granting us their permission to use the data. We thank Benoît Nauleau and Denis Paquet for their technical support. We thank Patrick Meynier for his support in the acquisition of the VSP data. We thank Pierre Gaudiani for the acquisition of full waveform acoustic data.

References

- [1] Mari J.L., Porel G., 2007, 3D seismic imaging of a near – surface heterogeneous aquifer: a case study, *Oil and Gas Science and Technology, Rev IFP* 63, 179-201. doi: 10.2516/ogst/2007077.
- [2] Bernard S., Delay F., Porel G., 2006, A new method of data inversion for the identification of fractal characteristics and homogenization scale from hydraulic pumping tests in fractured aquifers. *Journal of Hydrology* 328, 647-658.

- [3] Kaczmaryk A., Delay F., 2007a, Interpretation of interference pumping tests in fractured limestone by means of dual-medium approaches. *Journal of Hydrology* 337, 133-146. doi: 10.1016/j.jhydrol.2007.01.004.
- [4] Kaczmaryk A., Delay F., 2007b, Improving dual-porosity-medium approaches to account for karstic flow in a fractured limestone. Application to the automatic inversion of hydraulic interference tests. *Journal of Hydrology* 347, 391-403. doi: 10.1016/j.jhydrol.2007.09.037.
- [5] Bourbiaux B., Callot J.P., Doligez B., Fleury M., Gaumet F., Guiton M., Lenormand R., Mari J.L., Pourpak H., 2007, Multi-Scale Characterization of a Heterogeneous aquifer through the Integration of Geological, Geophysical and Flow Data: A Case Study, *Oil and Gas Science and Technology, Rev IFP* 61, 347-373.
- [6] Mari J.L., Delay F., 2011, Contribution of Seismic and acoustic methods to reservoir model building, in "Hydraulic Conductivity / Book 1", ISBN 978-953-307-288-3, InTech-Open Access Publisher, DOI: 10.5772/22051.
- [7] Mari J.L., Mendes M., 2012, High resolution near surface imaging of fracture corridors and cavities by combining Plus Minus method and refraction tomography, *Near Surface Geophysics* 10, 185-195, DOI: 10.3997/1873-0604.2011052.
- [8] Hagedoorn G.J., 1959, The Plus–Minus method of interpreting seismic refraction sections, *Geophysical Prospecting* 7, 158-182.
- [9] Mari J.L., Porel G., Bourbiaux B., 2009, From 3D Seismic to 3D Reservoir Deterministic Model Thanks to Logging Data: the Case Study of a Near Surface Heterogeneous Aquifer, *Oil and Gas Science and Technology, Rev IFP* 64, 119-131. DOI: 10.2516/ogst/2008049.
- [10] Faust L.Y., 1953, A velocity function including lithologic variation, *Geophysics* 18, 271-288.
- [11] Archie G. E., 1942, The electrical resistivity log as an aid in determining some reservoir characteristics, *Petroleum Technology* 146, 54-62.
- [12] Aslanyan A., Davydov D., 2012, Spectral Noise Logging, SNL-6, Technical overview, TGT Oilfield Services, www.tgtoil.com
- [13] Mari J.L., Porel G., 2016, Flow detection using well seismic data, Tu P2 02, 78th EAGE Conference & Exhibition, Vienna, Austria, 30 May-2 June.
- [14] Mari J.L., Porel G., 2015, Automated karstic reservoir analysis utilizing attributes, We N117 02, 77th EAGE Conference & Exhibition, Madrid IFEMA, Spain, 1-4 June.